Journal of Hepatocellular Carcinoma

Dovepress
Taylor & Francis Group

Open Access Full Text Article

ORIGINAL RESEARCH

Application of Intravoxel Incoherent Motion in the Prediction of Intra-Tumoral Tertiary Lymphoid Structures in Hepatocellular Carcinoma

Lidi Ma[1,2,*], Shuting Liao[1,2,*], Xiaolan Zhang[3,*], Fan Zhou[1,2,*], Zhijun Geng[1,2,*], Jing Hu[3], Yunfei Zhang[4], Cheng Zhang[1,2], Tiebao Meng[1,2], Shutong Wang[5], Chuanmiao Xie[1,2]

[1]Collaborative Innovation Center for Cancer Medicine, State Key Laboratory of Oncology in South China, Guangdong Provincial Clinical Research Center for Cancer, Sun Yat-Sen University Cancer Center, Guangzhou, 510060, People's Republic of China; [2]Department of Radiology, Sun Yat-sen University Cancer Center, State Key Laboratory of Oncology in South China, Guangzhou, People's Republic of China; [3]Shukun Technology Co., Ltd, Beijing, People's Republic of China; [4]Central Research Institute, United Imaging Healthcare, Shanghai, People's Republic of China; [5]Center of Hepato-Pancreato-Biliary Surgery, the First Affiliated Hospital, Sun Yat-Sen University, Guangzhou, Guangdong, 510080, People's Republic of China

*These authors contributed equally to this work

Correspondence: Chuanmiao Xie, Department of Radiology, Sun Yat-sen University Cancer Center, Guangzhou, 510060, People's Republic of China, Email xchuanm@sysucc.org.cn; Shutong Wang, Center of Hepato-Pancreato-Biliary Surgery, Center of Hepato-Pancreato-Biliary Surgery, the First Affiliated Hospital, Sun Yat-sen University, Guangzhou, Guangdong, 510080, People's Republic of China, Email wangsht23@mail.sysu.edu.cn

Objective: To explore the value of intravoxel incoherent motion (IVIM) sequences in predicting intra-tumoral tertiary lymphoid structures (TLSs).

Materials and Methods: This prospective study pre-operatively enrolled hepatocellular carcinoma (HCC) patients who underwent magnetic resonance imaging including IVIM sequences, between January 2019 and April 2021. Intra-tumoral TLSs presence was assessed on pathological slide images. Clinical and radiological characteristics were collected. IVIM quantitative parameters and radiomics features were obtained based on the whole delineated tumor volume. By using feature selection techniques, 22 radiomics features, clinical-radiological features (lymphocyte count and satellite nodules), and IVIM parameters (apparent diffusion coefficient (ADC_90Percentile), perfusion fraction (f_Maximum)) were selected. The logistic regression algorithm was used to construct the prediction model based on the combination of these features. The diagnostic performance was assessed using the area under the receiver operating characteristic (AUC). The recurrence-free survival (RFS) was evaluated with Kaplan–Meier curves.

Results: A total of 168 patients were divided into training (n=128) and testing (n=40) cohorts (mean age: 56.83±14.43 years; 149 [88.69%] males; 130 TLSs+). In testing cohort, the model combining multimodal features demonstrated a good performance (AUC: 0.86) and significantly outperformed models based on single-modality features. The model based on radiomics features (AUC: 0.80) had better performance than other features, including IVIM parameter maps (ADC_90Percentile and f_Maximum, AUC: 0.72) and clinical-radiological characteristics (satellite nodules and lymphocyte counts, AUC: 0.59). TLSs+ patients had higher RFS than TSLs- patients (all $p < 0.05$).

Conclusion: The nomogram based on the proposed model can be used as a pre-operative predictive biomarker of TLSs.

Critical Relevance Statement: The nomogram incorporating IVIM sequences may serve as a pre-operative predictive biomarker of intra-tumoral tertiary lymphoid structure (TLS) status.

Keywords: intravoxel incoherent motion, tertiary lymphatic structures, hepatocellular carcinoma, radiomics, recurrence-free survival

Introduction

Primary liver cancer is the second largest contributor to cancer-related mortality, with hepatocellular carcinoma (HCC) accounting for 80–90% of cases.[1] The outcome for patients with early HCC post-surgery remains unsatisfactory, as recurrence is observed in 70% of cases within five years.[2] Although immune checkpoint blockade immunotherapy shows promise in treating advanced HCC, its varying objective response rates across individuals remain a major obstacle.[3]

Received: 24 November 2024
Accepted: 14 February 2025
Published: 22 February 2025

In recent years, tertiary lymphatic structures (TLSs) have attracted particular interest in prognosis of HCC. TLSs are lymphoid aggregates in non-lymphoid tissues that result from persistent and unresolved inflammatory processes, including infection, autoimmune disease, and cancer.[4,5] Intra-tumor TLSs have shown a positive correlation with a decreased likelihood of tumor recurrence and improved overall survival rates across several solid malignancies.[6,7] Furthermore, intra-tumor TLSs have been proven to be associated with postoperative recurrence-free survival (RFS), and enhanced immunotherapy response in HCC.[8,9] However, the presence of TLSs can only be confirmed via postoperative pathological and immunohistochemical evaluation.[8,10] Therefore, it would be highly beneficial to develop a noninvasive and easily feasible method for determining the presence of TLSs.

Medical imaging plays a significant role in the diagnosis of HCC. HCC can be diagnosed based on typical imaging features. Tumors with heterogeneity, such as different histopathologic characteristics, and immune cell infiltration may exhibit different imaging features.[11,12] A previous study demonstrated that qualitative imaging features on pre-operative computed tomography (CT) may be predictors of intra-tumor TLSs in HCC, suggesting a possibility to infer TLS status through image-derived morphometrics.[13] However, qualitative analysis is limited by inconsistencies in subjective interpretation.

Diffusion weighted imaging (DWI) is a noninvasive technique used for evaluating the molecular diffusion of water, without the use of a contrast agent. Compared with the apparent diffusion coefficient (ADC) calculated by a monoexponential model, multi-b-value DWI with intravoxel incoherent motion (IVIM) can evaluate the true molecular diffusion and the blood microcirculation perfusion by using multi-b-values in a bi-exponential model. IVIM is capable of analyzing non-Gaussian diffusion and can more accurately describe the heterogeneity of tumor components.[14]

IVIM-derived parameters have shown great promise in detecting HCC, including differentiating HCC from intrahepatic cholangiocarcinoma[15] and benign tumors, identifying the histologic grade, predicting microvascular invasion (MVI) and prognosis, and evaluating liver regeneration and efficacy of response to interventional therapy.[16–21] However, no previous studies have focused on the relationship between the IVIM parameters and TLSs; consequently, whether the quantitative parameters of IVIM can predict TLSs remains unknown. Therefore, this study aimed to determine the effectiveness of IVIM parameters and conventional radiologic characteristics in the pre-operative prediction of TLSs in HCC, as well as their prognostic implications.

Methods

Participants

This prospective study was approved by the ethics committee of Sun-Yat Sen University Cancer Center (Approval Number: B2019-187-01) and followed the Declaration of Helsinki. Written informed consent was obtained from all the participants. Overall, 695 consecutive patients with suspected HCC who underwent pre-operative routine MR (T1-weighted imaging (T1WI), T2-weighted imaging (T2WI) and enhanced sequences based on T1WI) and IVIM sequence examination between January 30, 2019, and April 1, 2021, were eligible for inclusion. The inclusion criteria were as follows: age $\geq$ 18 years; a clinically suspected diagnosis of HCC; and without biopsy prior to magnetic resonance imaging (MRI) examination. The exclusion criteria were as follows: pathologically confirmed malignancies that were not HCC (n=356); history of receiving anti-tumor therapy before hepatectomy (n=52); Barcelona Clinic Liver Cancer (BCLC) stage C (n=19); lesion size <10 mm (n=38); and poor image quality in the IVIM acquisition (n=22) or incomplete data (n=40). In total, 168 patients with HCC were enrolled in this study, independently divided into the training cohort (n=128, from January 2019 to November 2020) and internal independent testing cohort (n=40, from December 2020 to April 2021) at a ratio of 3:1 through temporal partitioning. When it comes to patients had multiple lesions, only the largest HCC lesion was included in the analysis. Figure 1 illustrates the patient recruitment process.

Histopathological Analysis

The hematoxylin-eosin stained whole pathological slide images (WSIs) of each patient were reviewed by an experienced pathologist. The presence of intra-tumoral TLSs was assessed morphologically on the WSIs (Figure 2A-C). TLSs were classified as aggregates (Aggregates, Figure 2A) and lymphoid follicles (FL). FL were further divided into primary

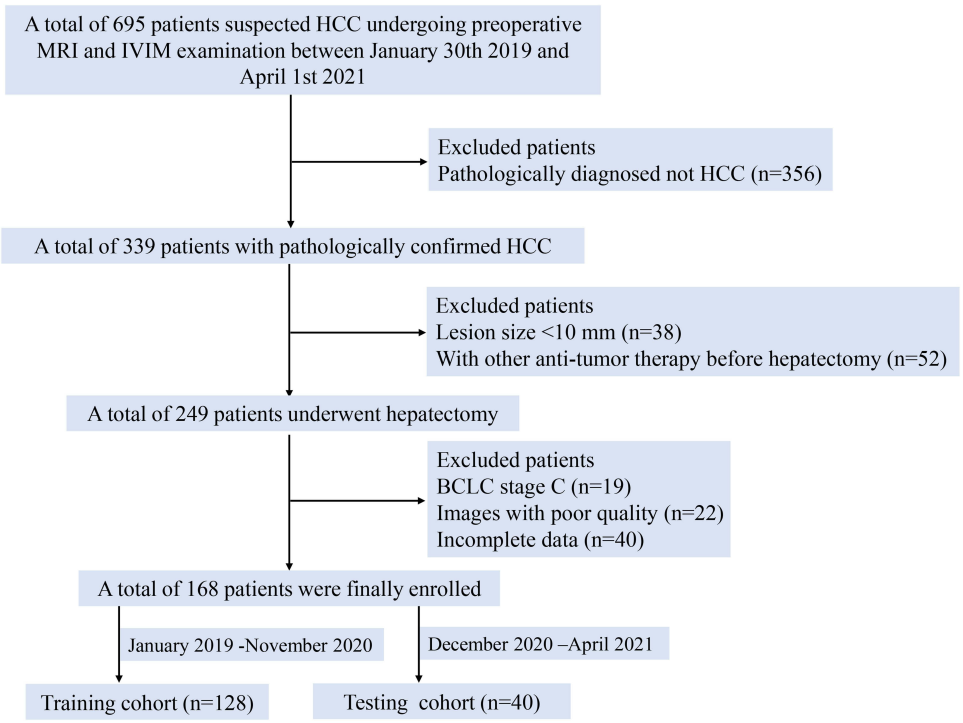

Figure 1 Flow chart of the study population.
Abbreviations: HCC, hepatocellular carcinoma; IVIM, intravoxel incoherent motion; BCLC, Barcelona Clinic Liver Cancer.

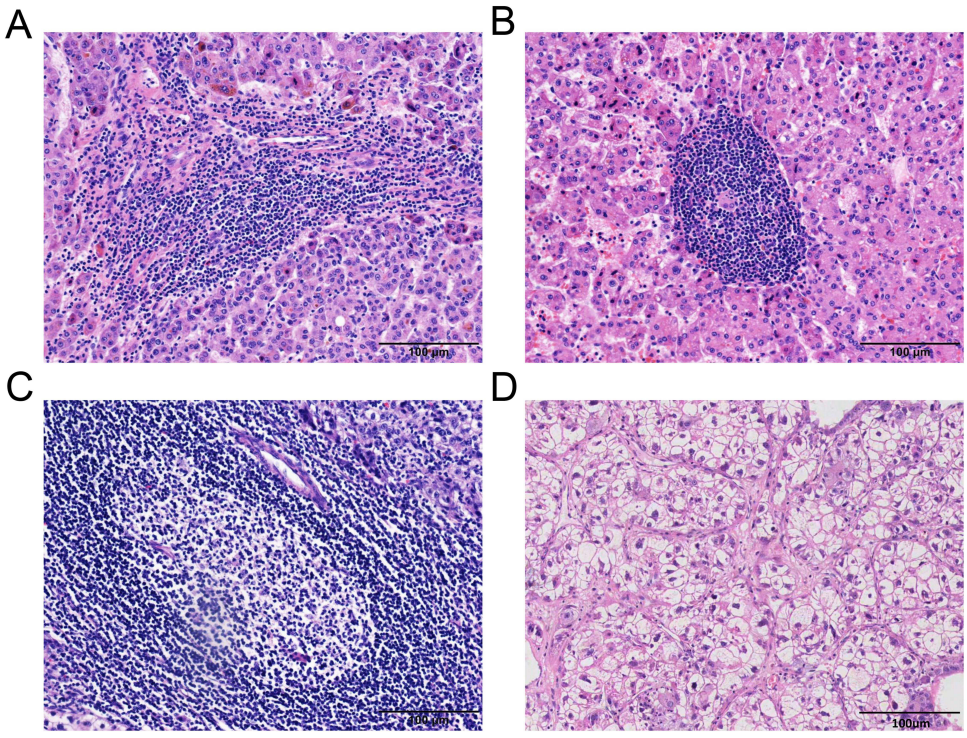

Figure 2 Representative morphological features of intra-tumoral tertiary lymphoid structures. (**A**) Aggregates. (**B**) Primary lymphoid follicles (FL). (**C**) Secondary follicles. (**D**) Patients without intra-tumoral TLSs.

https://doi.org/10.2147/JHC.S508357

follicles (FL-I, Figure 2B) and secondary follicles (FL-II, Figure 2C), based on the maturation stage of the TLSs.[22] The tumors were classified as TLSs+ (presence of Aggregates or FL) or TLSs- (absence of Aggregates and FL, Figure 2D).

MRI Acquisition

All MRI examinations were performed using a 3.0-T MR system (United Imaging, uMR780). IVIM diffusion-weighted imaging (repetition time/echo time, 4582 ms /67.1 ms; matrix, 160 × 118; slice thickness, 5 mm; field of view, 236 mm × 320 mm; and spacing between slices, 6 mm) was performed using eight b-values, ranging from 0–800 s/mm^2 (0, 20, 40, 80, 100, 200, 500, and 800 s/mm^2). The standardized scanning protocol comprised several routine MR imaging sequences with extracellular agents (dose, 0.1 mL/kg; injection rate, 2.0–3.0 mL/s), namely the respiratory-triggered axial T2-weighted imaging, in and out phase T1-weighted imaging, and pre-and post-contrast liver acceleration volume acquisition (including arterial phase [20s], portal venous phase [60s], and delayed phase [180s]). Table S1 presents the parameters of each sequence.

Clinical Characteristics and Radiologic Assessment

The demographic and laboratory characteristics were extracted from the electronic medical records, including age, sex, hepatitis B status, α-fetoprotein (AFP), aspartate transaminase, alanine transaminase, alkaline phosphatase, lactate dehydrogenase, total bilirubin, albumin, and γ-glutamyl transpeptidase levels, white blood cell count, neutrophil counts (NEUT), lymphocyte counts (LYM), platelet count, Barcelona Clinic Liver Cancer (BCLC) stage, and pathological characteristics including MVI and cirrhosis.

The radiologic features were evaluated independently by two experienced radiologists blinded to the TLS status. The qualitatively evaluated radiologic features were as follows: maximum tumor diameter, tumor number, tumor margin, enhancement pattern, tumor capsule, peritumoral enhancement, satellite nodules, internal artery, boundary of tumor enhancement, tumor necrosis, and intra-tumoral hemorrhage. Table S2 delineates the aforementioned features. A consensus was reached via discussion in the case of disagreements between the two radiologists.

IVIM Parameters Extraction

All IVIM-DWI images were transferred to a workstation (Diffusion-Weighted Imaging Kit, United Imaging Healthcare) for postprocessing. The quantitative pixelwise parameters derived from IVIM were obtained through the following fitting model:

$$S_b/S_0 = (1-f)\exp(-bD) + f \cdot \exp(-bD*)$$

where S_0 and S_b are, respectively, the signal intensity when a b value of 0 s/mm2 and other b values are applied. The bi-exponential model generated the ADC, true diffusion coefficient (Dt), perfusion-related diffusion coefficient (Dp), and perfusion fraction (f) maps. Radiologists 1 and 2 manually drew the volume of interests (VOIs) of the tumors within the visible borders, while avoiding the blood vessels. ITK-SNAP software (www.itksnap.org) was used to draw VOIs on the axial b-800 images of DWI-IVIM sequences, with reference to T2WI or contrast-enhanced images. The ADC, Dt, Dp, and f values (90 percentile,[14] maximum, mean, and skewness) were calculated using the parametric maps with the outlined VOIs. Subsequently, the IVIM parameters obtained by the two radiologists were averaged and subjected to univariate and multivariate logistic analyses for feature selection.

Radiomics Feature Extraction

The 6752 radiomics features were initially calculated on the ADC, Dt, Dp, and f maps through PyRadiomics (version 3.1.0),[23] including shape, first-order features, gray level dependence matrix, gray level size zone matrix, gray level co-existence matrix, and gray-level run-length matrix. Then, the intra-class correlation coefficient (ICC) was calculated to determine the inter-observer consistency of the extracted features, and 2667 radiomics features with ICC value >0.75 were included in the subsequent analysis. In the next, radiomics features were screened using Pearson correlation tests, and 849 features were retained after univariable Pearson correlation coefficient (PCC >0.9). Finally, twenty-two features

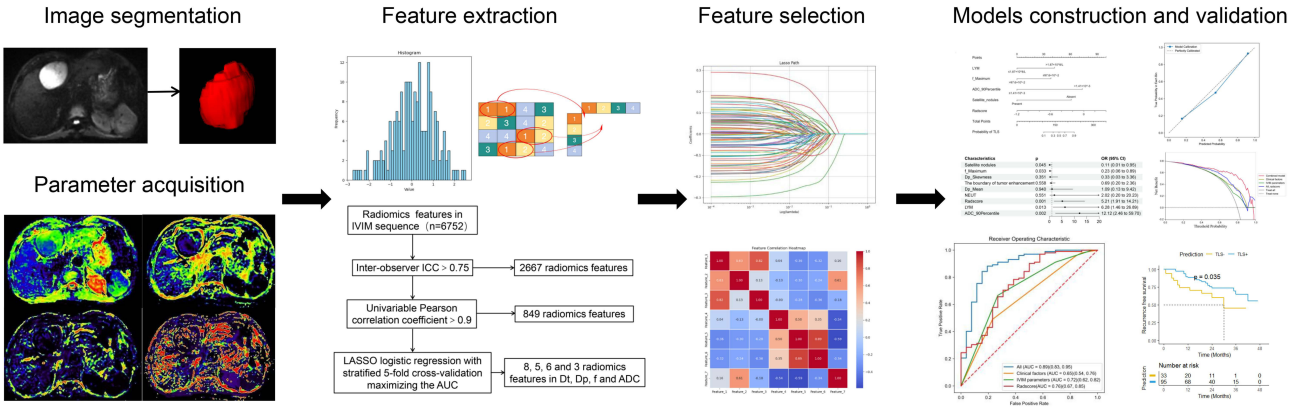

Figure 3 Flowchart depicting the acquisition of the IVIM-DWI and radiomics parameters and model construction.
Abbreviations: IVIM, intravoxel incoherent motion; DWI, diffusion-weighted imaging.

were identified and used to calculate the radscore by using the Least Absolute Shrinkage and Selection Operator (LASSO), comprising eight, five, six, and three radiomics features from the Dt, Dp, f, and ADC, respectively (Table S3).

Model Construction

Logistic regression analysis was utilized to construct the model based on a combination of significant factors, including IVIM parameters, clinical-radiological characteristics, and the rad-score. Figure 3 illustrates the process of model acquisition and construction. The model's performance within the training cohort was rigorously assessed using a five-fold cross-validation method. Subsequently, the models were retrained on the entire training cohort, and their effectiveness was evaluated in the testing cohort.

For comparative analysis, separate models were developed using individual features: radiomics, IVIM parameters, and clinical features, respectively. This approach allowed for a comprehensive evaluation of each feature set's relative contributions to the model's predictive power.

Follow-Up

RFS was defined as the end point from the date of liver resection to the date of initial tumor recurrence or the last follow-up date. All patients were followed up after liver resection, and serum AFP level measurements, contrast-enhanced ultrasound, and CT or MRI examinations were conducted every 2–3 months. Patients who did not experience recurrence or death at the time of data analysis were censored as alive and event-free on the date of the last follow-up visit (August 1, 2023).

Statistical Analysis

The chi-squared test or Fisher's exact test and independent t-tests or Mann–Whitney *U*-tests were used to compare the categorical and quantitative variables, respectively. The Kolmogorov–Smirnov test was used to test the normality of the quantitative variables. The ICC and Cohen's kappa were used to determine the intra-observer reliability for continuous and categorical variables, respectively. Continuous variables were transformed into binary variables based on clinical reference values or the optimal cut-off using Youden's index for univariate and multivariate logistic regression analyses. Backward stepwise regression was used in the multivariate logistic regression. Diagnostic accuracy was quantified via the area under the receiver operating curve (AUC) analysis. The cut-off values for the IVIM parameters, radscore, and nomogram were determined using the maximum Youden index of the ROC. The accuracy, sensitivity, specificity, positive predictive value, and negative predictive value of the model were calculated. The predictions of models were compared using the DeLong test. Calibration curves of the nomogram were plotted to assess the consistency between prediction and observation via the Hosmer–Lemeshow test. Decision curve analysis (DCA) was performed to evaluate clinical utility. The Kaplan–Meier method with the Log rank test was used to create the survival analyses of the TLS status and

https://doi.org/10.2147/JHC.S508357

nomogram. All statistical analyses were performed using Python (version 3.11.4) and R (version 4.2.2). All *p*-values were two-sided, and statistical significance was set at $p < 0.05$.

Results

Patient Characteristics

This study enrolled 128 patients in the training cohort (TLSs+: 102, TLSs-: 26; 115 [89.80%] males; age: 54.47±10.90 years) and 40 patients in the testing cohort (TLSs+: 28, TLSs-: 12; 34 [85%] males, age: 55.67±10.45 years). There was no statistical difference in regarding positive ratio of TLSs between the training and testing cohort ($p = 0.288$). The

Table 1 Baseline Patient Characteristics

Characteristic	Training Cohort			Testing Cohort		
	TLSs (-)	TLSs (+)	*P* value	TLSs (-)	TLSs (+)	*P* value
	N=26	N=102		N=12	N=28	
Age	56.70 (13.00)	53.90 (10.30)	0.325	56.20 (11.40)	55.50 (10.40)	0.857
Gender			1			0.648
Male	24 (92.31%)	91 (89.22%)		11 (91.67%)	23 (82.14%)	
Female	2 (7.69%)	11 (10.78%)		1 (8.33%)	5 (17.86%)	
MVI status			0.561			0.139
Negative	21 (80.77%)	73 (71.57%)		8 (66.67%)	25 (89.29%)	
Positive	5 (19.23%)	29 (28.43%)		4 (33.33%)	3 (10.71%)	
Cirrhosis			0.91			1
Negative	17 (65.40%)	63 (61.80%)		8 (66.67%)	18 (64.29%)	
Positive	9 (34.60%)	39 (38.20%)		4 (33.33%)	10 (35.71%)	
HBsAg			1			0.57
Negative	4 (15.38%)	15 (14.71%)		2 (16.67%)	2 (7.14%)	
Positive	22 (84.62%)	87 (85.29%)		10 (83.33%)	26 (92.86%)	
AFP (ng/mL)	40.20 [6.39;134]	32.71 [4.64;402]	1	31.50 [4.80;132]	206 [14.20;594]	0.082
ALB (g/L)	44.10 (2.94)	44.10 (3.27)	0.961	42.70 [38.80;44.40]	44.00 [41.40;45.50]	0.434
TBIL (umol/L)	15.10 [11.20;20.00]	12.80 [9.80;16.10]	0.056	15.40 [12.20;17.30]	11.90 [9.00;15.50]	0.148
WBC (10^9/L)	5.71 [4.90;6.88]	6.14 [4.96;6.82]	0.519	6.42 [5.75;7.70]	5.87 [5.18;6.35]	0.087
NEUT (10^9/L)	3.22 [2.82;4.34]	3.44 [2.78;4.06]	0.913	3.52 [3.24;4.54]	3.50 [2.94;4.12]	0.555
LYM (10^9/L)	1.65 [1.37;1.90]	1.87 [1.50;2.28]	0.066	2.00 (0.42)	1.77 (0.50)	0.148
NLR	2.21 [1.57;2.87]	1.67 [1.40;2.35]	0.047	1.73 [1.48;2.79]	2.12 [1.64;2.64]	0.516
PLT (10^9/L)	178 [144;212]	184 [142;226]	0.955	204 (67.00)	195 (46.70)	0.663
ALT (U/L)	33.30 [23.70;43.00]	30.40 [21.90;45.20]	0.903	30.00 [21.60;51.10]	33.50 [22.70;52.00]	0.637
AST (U/L)	31.10 [24.80;38.70]	28.10 [21.90;37.60]	0.617	36.00 [31.30;46.90]	28.00 [24.90;39.80]	0.108
ALP (U/L)	87.00 [66.40;103]	80.20 [63.90;95.80]	0.400	97.50 [80.80;105]	72.30 [61.90;90.20]	0.105
GGT (U/L)	54.90 [33.00;72.90]	47.10 [32.50;82.40]	0.754	60.30 [43.90;83.90]	45.30 [35.20;62.40]	0.098
LDH (U/L)	181 [165;216]	174 [153;209]	0.273	186 [164;214]	181 [167;204]	0.768
Location			0.485			0.404
Left lobe	10 (38.46%)	29 (28.43%)		3 (25.00%)	10 (35.71%)	
Right lobe	15 (57.69%)	63 (61.76%)		8 (66.67%)	18 (64.29%)	
Bilateral lobe	1 (3.85%)	10 (9.80%)		1 (8.33%)	0 (0.00%)	
Number			0.734			0.298
Single	24 (92.31%)	90 (88.24%)		12 (100%)	23 (82.14%)	
Multiple	2 (7.69%)	12 (11.76%)		0 (0.00%)	5 (17.86%)	
Maximum tumor diameter(mm)	45.50 [26.80;54.50]	35.00 [26.00;51.80]	0.349	56.00 [43.50;69.00]	29.00 [22.00;47.00]	0.001
Intratumoral hemorrhage			0.153			0.627
Negative	19 (73.08%)	87 (85.29%)		10 (83.33%)	25 (89.29%)	
Positive	7 (26.92%)	15 (14.71%)		2 (16.67%)	3 (10.71%)	
Necrosis			0.145			0.016

(*Continued*)

Table 1 (Continued).

Characteristic	Training Cohort			Testing Cohort		
	TLSs (-)	TLSs (+)	*P* value	TLSs (-)	TLSs (+)	*P* value
	N=26	N=102		N=12	N=28	
Negative	10 (38.46%)	58 (56.86%)		2 (16.67%)	18 (64.29%)	
Positive	16 (61.54%)	44 (43.14%)		10 (83.33%)	10 (35.71%)	
AP enhancement type			0.116			1
Without APHE	3 (11.54%)	3 (2.94%)		12 (100%)	27 (96.43%)	
Nonrim APHE	23 (88.46%)	94 (92.16%)		0 (0.00%)	1 (3.57%)	
Rim APHE	0 (0.00%)	5 (4.90%)		0 (0.00%)	0 (0.00%)	
Nonperipheral washout			0.694			1
Absent	3 (11.54%)	8 (7.84%)		0 (0.00%)	1 (3.57%)	
Present	23 (88.46%)	94 (92.16%)		12 (100%)	27 (96.43%)	
Capsule appearance			0.423			0.39
Absent	8 (30.80%)	37 (36.30%)		5 (41.67%)	12 (42.86%)	
Complete	5 (19.20%)	28 (27.50%)		2 (16.67%)	1 (3.57%)	
Incomplete	13 (50.00%)	37 (36.30%)		5 (41.67%)	15 (53.57%)	
Satellite nodules			0.089			0.298
Negative	22 (84.60%)	98 (96.10%)		12 (100%)	23 (82.14%)	
Positive	4 (15.40%)	4 (3.92%)		0 (0.00%)	5 (17.86%)	
Tumor margin			0.371			0.564
Smooth margin	2 (7.69%)	20 (19.60%)		0 (0.00%)	4 (14.29%)	
Nodular with extranodular extension	16 (61.50%)	51 (50.00%)		8 (66.67%)	18 (64.29%)	
Multinodular confluent	4 (15.40%)	21 (20.60%)		3 (25.00%)	5 (17.86%)	
Infiltrative shaped tumor	4 (15.40%)	10 (9.80%)		1 (8.33%)	1 (3.57%)	
Internal artery			0.722			0.091
Negative	16 (61.50%)	69 (67.60%)		5 (41.67%)	20 (71.43%)	
Positive	10 (38.50%)	33 (32.40%)		7 (58.33%)	8 (28.57%)	
AP peritumoral enhancement			0.466			0.729
Negative	18 (69.20%)	80 (78.40%)		8 (66.67%)	16 (57.14%)	
Positive	8 (30.80%)	22 (21.60%)		4 (33.33%)	12 (42.86%)	
Boundary of the tumor enhancement			0.053			0.112
Clear	14 (53.85%)	77 (75.49%)		10(83.33%)	16(57.14%)	
Obscure	12(46.15%)	25 (24.51%)		2(16.67%)	12(42.86%)	
BCLC stage			0.332			0.039
0	4 (15.40%)	12 (11.80%)		0(0%)	5(17.86%)	
A	18 (69.20%)	82 (80.40%)		12(100%)	17(60.71%)	
B	4 (15.40%)	8 (7.84%)		0(0%)	6(21.42%)	
Dt_90Percentile (10^-3)	1.06 (0.29)	1.05 (0.29)	0.847	1.07 [0.97;1.17]	1.03 [0.94;1.28]	1
Dt_Maximum (10^-3)	2.23 [1.79;2.84]	2.26 [1.71;2.74]	0.840	3.20 [2.42;5.16]	1.94 [1.75;2.57]	0.001
Dt_Mean (10^-3)	0.56 (0.22)	0.55 (0.21)	0.826	0.64 (0.17)	0.59 (0.22)	0.429
Dt_Skewness (10^-3)	509 [78.20;1152]	626 [54.80;1359]	0.661	848 (1086)	543 (707)	0.384
Dp_90Percentile (10^-3)	100 [100;100]	100 [100;100]	0.957	100 [100;100]	100 [100;100]	1
Dp _Maximum (10^-3)	100 [100;100]	100 [100;100]	1	100 [100;100]	100 [100;100]	1
Dp_Mean (10^-3)	38.90 [30.70;51.00]	43.10 [34.60;51.70]	0.273	45.00 (10.20)	45.41 (10.14)	0.892
Dp_Skewness (10^-3)	523 [11.40;974]	410 [15.70;763]	0.359	203 [−72.71;479]	216 [−49.99;480]	0.768
f_90Percentile (10^-3)	571 [512;636]	577 [524;635]	0.981	568 (100)	578 (106)	0.774
f_Maximum (10^-3)	962 [887;984]	946 [887;975]	0.317	973 [935;988]	926 [877;966]	0.007
f_Mean (10^-3)	246 [217;294]	250 [212;295]	0.962	248 (89.50)	270 (67.20)	0.458
f_Skewness (10^-3)	567 [318;781]	581 [311;998]	0.481	778 (569)	417 (455)	0.068
ADC_90Percentile (10^-3)	1.65 [1.41;1.96]	1.67 [1.56;1.82]	0.722	1.69 (0.33)	1.76 (0.34)	0.559

(*Continued*)

https://doi.org/10.2147/JHC.S508357

Table 1 (Continued).

Characteristic	Training Cohort			Testing Cohort		
	TLSs (-)	TLSs (+)	*P* value	TLSs (-)	TLSs (+)	*P* value
	N=26	N=102		N=12	N=28	
ADC_Maximum (10^-3)	2.99 (0.69)	3.04 (0.66)	0.720	3.38 (0.43)	2.82 (0.65)	0.003
ADC_Mean (10^-3)	1.03 [0.87;1.21]	1.04 [0.86;1.14]	0.594	1.08 (0.27)	1.07 (0.25)	0.912
ADC_Skewness (10^-3)	110 [−143.75;367]	213 [−75.60;579]	0.241	414 (359)	9.28 (368)	0.004

Notes: For continuous variables, the mean ± SD is expressed in () if the variable is normally distributed, otherwise the median and IQR are expressed in [].
Abbreviations: MVI, microvascular invasion; AFP, α-fetoprotein; CEA, carcinoembryonic antigen; CA199, cancer antigen; PIVKA-II, vitamin K deficiency or antagonist- II; AST, aspartate transaminase; ALT, alanine transaminase; ALP, alkaline phosphatase; LDH, lactate dehydrogenase; GGT, γ-glutamyl transpeptidase; WBC, white blood cell count; NEUT, neutrophil counts; LYM, lymphocyte counts; NLR, neutrophil counts/lymphocyte counts; PLT, platelet count; TBIL, total bilirubin; ALB, albumin; AP, arterial phase; APHE, APHE, arterial phase hyperenhancement; DWI, diffusion weighted imaging; BCLC, Barcelona Clinic Liver Cancer; ADC, apparent diffusion coefficient; Dt, true diffusion coefficient; Dp, perfusion related diffusion coefficient; f, perfusion fraction.

patients' characteristics between the TLSs+ and TLSs- groups in the training and testing cohorts are presented in Table 1. The MVI grade (p = 0.561, 0.139), cirrhosis status (p = 0.910, 1), and HBsAg status (p = 1, 0.570) did not differ significantly between the groups in two cohorts.

Feature Selection

ROC analysis utilizing Youden's index or clinical reference values was used to determine the optimal threshold value of clinical continuous variables and IVIM parameters (Table 2). The IVIM parameters (ADC, Dt, and f mean values) did not differ significantly between the TLSs+ and TLSs- groups (p = 0.594, 0.826, and 0.962, respectively). Univariate logistic regression analysis revealed statistically significant correlations between the TLS status and ADC_90Percentile (odds ratio [OR], 4.59; 95% confidence interval [CI]: 1.56–13.49; p = 0.006), Dp_Mean (OR, 2.64; 95% CI: 1.08–6.45; p = 0.033), Dp_Skewness (OR, 0.35; 95% CI: 0.142–0.882; p = 0.026), and f_Maximum (OR, 0.38; 95% CI: 0.16–0.93; p = 0.033). Multivariate logistic regression analyses revealed that ADC_90Percentile (OR, 12.12; 95% CI: 2.46–59.70; p = 0.002) and

Table 2 Logistic Regression Analysis of Variables for Their Association with Tertiary Lymphatic Structures in Patients

Characteristic	Univariable Analysis		Multivariable Analysis	
	OR (95% CI)	*P* value	OR (95% CI)	*P* value
Age (≤53 years vs >53 years)	0.563(0.224,1.413)	0.221		
Gender (female vs male)	1.451(0.301,6.989)	0.643		
HBsAg (negative vs positive)	1.055(0.318,3.494)	0.931		
Cirrhosis (absent vs present)	0.855(0.347,2.106)	0.734		
MVI (absent vs present)	1.306(0.609,2.798)	0.493		
AFP (≤200 ng/mL vs >200 ng/mL)	1.594(0.585,4.343)	0.362		
ALB (≤55 g/L vs >55 g/L)	1(1,1)	/		
TBIL (≤20.5 umol/L vs >20.5 umol/L)	0.406(0.123,1.338)	0.139		
WBC (≤6.17×10^9/L vs >6.17×10^9/L)	2.250(0.898,5.639)	0.084		
NEUT (≤5.31×10^9/L vs >5.31×10^9/L)	0.216(0.057,0.816)	0.0234*	2.016(0.201,20.229)	0.551
LYM (≤1.87×10^9/L vs >1.87×10^9/L)	2.823(1.092,7.296)	0.032*	6.275(1.464,26.891)	0.013*
PLT (≤213×10^9/L vs>213×10^9/L)	1.594(0.585,4.343)	0.362		
ALT (≤50 U/L vs >50 U/L)	1.870(0.510,6.852)	0.345		
AST (≤40 U/L vs >40 U/L)	1.082(0.391,2.995)	0.879		
ALP (≤125 U/L vs >125 U/L)	0.833(0.212,3.275)	0.794		
GGT (≤60 U/L vs >60 U/L)	0.990(0.409,2.401)	0.983		
LDH (≤250 U/L vs >250 U/L)	1.842(0.216,15.674)	0.576		
Dt_90Percentile (≤0.884×10^-3/L vs >0.884×10^-3/L)	1.818(0.716,4.618)	0.209		
Dt_Maximum (≤3.330×10^-3/L vs >3.330×10^-3/L)	0.575(0.198,1.666)	0.308		
Dt_Mean (≤0.344×10^-3/L vs >0.344×10^-3/L)	0.503(0.138,1.837)	0.299		

(*Continued*)

Table 2 (Continued).

Characteristic	Univariable Analysis		Multivariable Analysis	
	OR (95% CI)	***P* value**	**OR (95% CI)**	***P* value**
Dt_Skewness (≤366.782×10^-3/L vs >366.782×10^-3/L)	1.641(0.686,3.927)	0.266		
Dp_90Percentile (≤100×10^-3/L vs >100×10^-3/L)	1.131(0.221,5.795)	0.883		
Dp_Maximum	1(1,1)	/		
Dp_Mean (≤34.621×10^-3/L vs >34.621×10^-3/L)	2.640(1.081,6.450)	0.033*	1.086(0.125,9.415)	0.940
Dp_Skewness (≤862.802×10^-3/L vs >862.802×10^-3/L)	0.354(0.142,0.882)	0.0258*	0.333(0.033,3.356)	0.351
f_90Percentile (≤533.6×10^-3 vs >533.6×10^-3)	1.652(0.670,4.070)	0.275		
f_Maximum (≤976.2×10^-3 vs >976.2×10^-3)	0.379(0.155,0.925)	0.033*	0.229(0.059,0.888)	0.033*
f_Mean (≤232.7×10^-3 vs >232.7×10^-3)	0.526(0.203,1.364)	0.186		
f_Skewness (≤924.3×10^-3 vs >924.3×10^-3)	3.194(0.891,11.447)	0.074		
ADC_90Percentile (≤1.414×10^-3/L vs >1.414×10^-3/L)	4.593(1.563,13.494)	0.006*	12.121(2.461,59.703)	0.002*
ADC_Maximum (≤2.391×10^-3/L vs >2.3911×10^-3/L)	2.316(0.824,6.512)	0.111		
ADC_Mean (≤1.178×10^-3/L vs >1.178×10^-3/L)	0.415(0.165,1.046)	0.062		
ADC_Skewness (≤269.489×10^-3/L vs >269.489×10^-3/L)	2.319(0.897,5.998)	0.083		
Radscore (continuous)	4.461(2.033,9.789)	<0.001*	5.213(1.912,14.214)	0.001*
Number (single vs multiple)	1.600(0.335,7.639)	0.556		
Maximum tumor diameter (≤50 mm vs >50 mm)	0.605(0.246,1.492)	0.275		
Intratumoral hemorrhage (absent vs present)	0.468(0.168,1.305)	0.147		
Necrosis (absent vs present)	0.474(0.196,1.145)	0.097		
Signal (homogeneity vs heterogeneity))	0.635(0.253,1.596)	0.334		
Nonperipheral_washout (absent vs present)	1.533(0.377,6.234)	0.551		
Satellite nodules (absent vs present)	0.224(0.052,0.968)	0.045*	0.106(0.012,0.948)	0.045*
Internal artery (absent vs present)	0.765(0.313,1.868)	0.557		
AP peritumoral enhancement (absent vs present)	0.619(0.238,1.611)	0.326		
Boundary of the tumor enhancement (clear vs obscure)	0.379(0.155,0.925)	0.033*	0.694(0.205,2.356)	0.558
Location	1.185(0.494,2.840)	0.704		
Capsule appearance (absent vs present)	1.589(0.546,4.623)	0.395		
AP enhancement type (nonrim APHE)	1.533(0.377,6.234)	0.551		
Tumor margin (smooth vs nonsmooth)	0.792(0.486,1.290)	0.348		
BCLC stage (0 vs A vs B)	0.835(0.330,2.108)	0.702		

Notes: AFP, ALB, TBIL, ALT, AST, ALP, GGT, LDH, and maximum tumor diameter were classified using clinical reference values. The other variables were used to determine the optimal cut-off using Youden's index. *Data are statistically significant associations for identifying TLS status.

Abbreviations: MVI, microvascular invasion; AFP, α-fetoprotein; CEA, carcinoembryonic antigen; CA199, cancer antigen; PIVKA-II, vitamin K deficiency or antagonist- II; AST, aspartate transaminase; ALT, alanine transaminase; ALP, alkaline phosphatase; LDH, lactate dehydrogenase; GGT, γ-glutamyl transpeptidase; WBC, white blood cell count; NEUT, neutrophil counts; LYM, lymphocyte counts; NLR, neutrophil counts/lymphocyte counts; PLT, platelet count; TBIL, total bilirubin; ALB, albumin; AP, arterial phase; APHE, APHE, arterial phase hyperenhancement; DWI, diffusion weighted imaging; BCLC, Barcelona Clinic Liver Cancer; ADC, apparent diffusion coefficient; Dt, true diffusion coefficient; Dp, perfusion related diffusion coefficient; f, perfusion fraction.

f_Maximum (OR, 0.23; 95% CI: 0.06–0.89; $p = 0.033$) showed statistically significant associations for identifying TLS status. The optimal cut-off values of ADC_90Percentile and f_Maximum were 1.414×10^{-3}/L, 97.62% respectively (Table 2).

For the clinical and radiologic features, satellite nodules (OR, 0.22; 95% CI: 0.05–0.97; $p = 0.045$), boundary of tumor enhancement (OR, 0.38; 95% CI: 0.16–0.93; $p = 0.033$), NEUT (OR, 0.22; 95% CI: 0.06–0.82; $p = 0.024$), and LYM (OR, 2.82; 95% CI: 1.09–7.30; $p = 0.032$) showed significant associations with the TLS status through univariate logistic regression. Multivariate logistic regression analyses revealed that satellite nodules (OR, 0.11; 95% C: 0.01–0.95; $p = 0.045$) and LYM (OR: 6.28; 95% CI: 1.46–26.89; $p = 0.013$) showed statistically significant associations for identifying TLS status. The optimal cut-off value of LYM was 1.87×10^{8}/L (Table 2).

For the radiomics features, multivariate logistic regression analyses revealed that the total radscore differed significantly between the TLSs+ group and TLSs- group (OR, 5.21; 95% CI: 1.91–14.21; $p = 0.001$), which indicated that the radscore of the TLSs+ group was significantly higher than that of the TLSs- group.

Diagnostic Performance of the Models

The proposed method achieved favorable results across both training and testing cohorts. The average AUC value following the five-fold cross-validation was 0.88 (95% CI: 0.82, 0.94) (Figure 4A). The model's consistent performance across each fold of cross-validation indicates a low risk of overfitting. Furthermore, the model achieved an AUC of 0.86 in the testing cohort (Figure 4C). The variables incorporated in the model were constructed and presented as a nomogram and forest plot to facilitate personalized probability estimations and illustrate the significance of individual characteristics (Figure 5A and B). The calibration curves and DCA curves of the nomogram indicated good performance for model

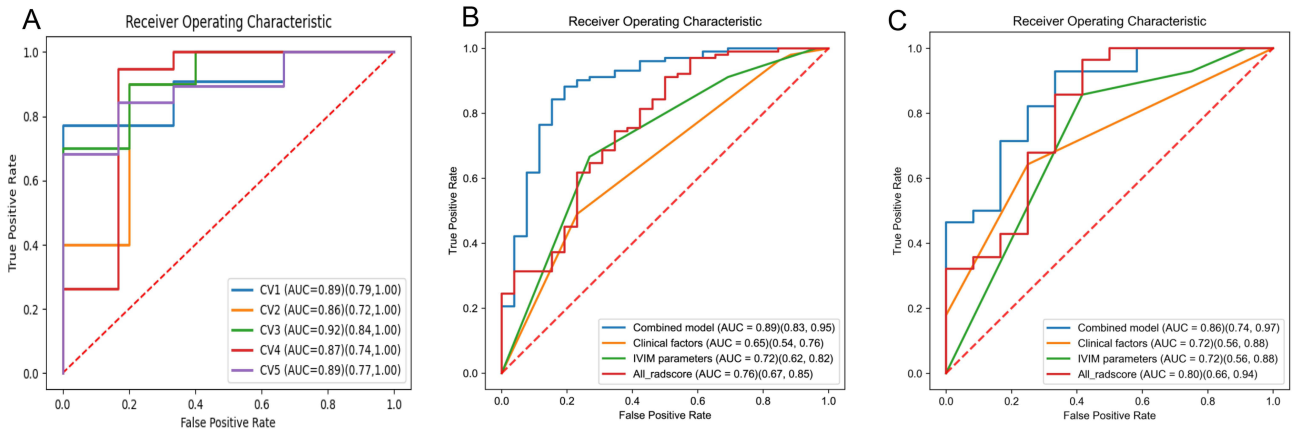

Figure 4 Assessment of the ability of the models to predict intra-tumoral tertiary lymphoid structures. (**A**) The receiver operating characteristic (ROC) curve of the combined model based on a five-fold cross-validation. (**B**) ROC of different models in the training cohort. (**C**) ROC of different models in the testing cohort.

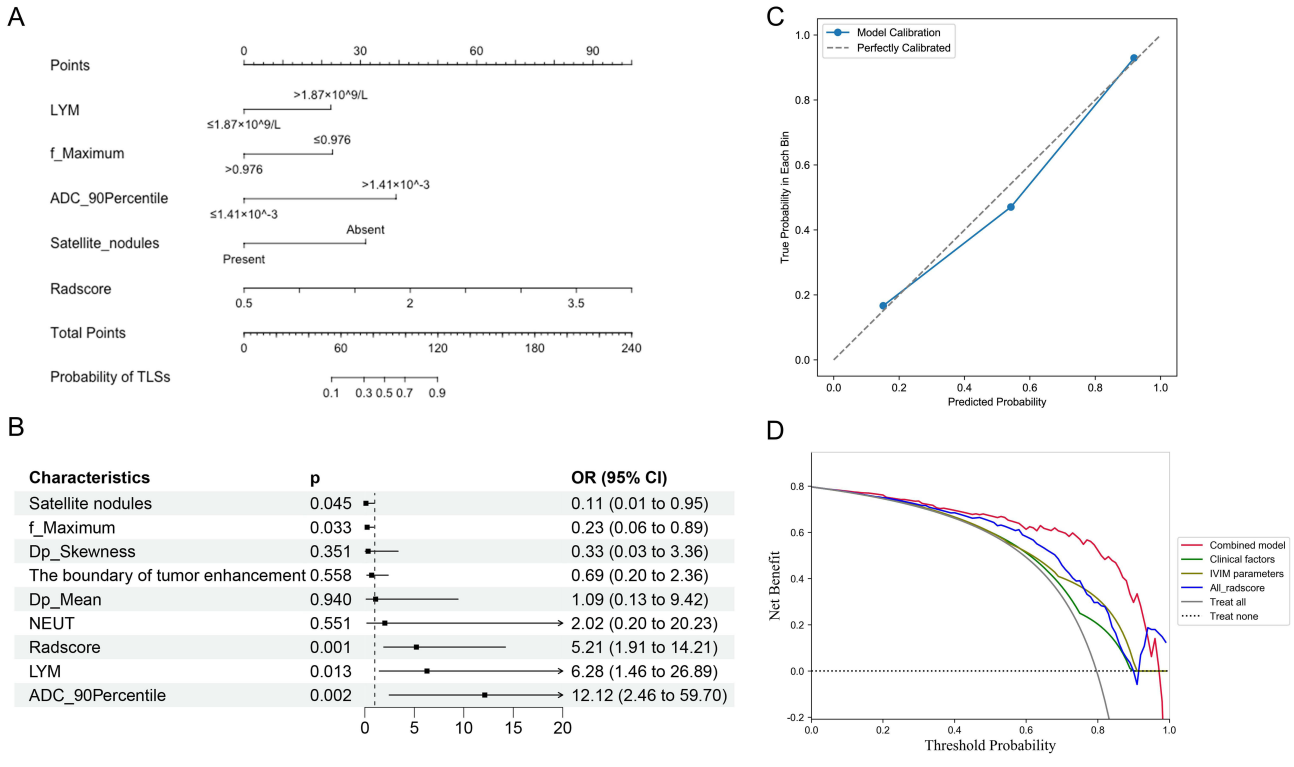

Figure 5 Construction and performance of the combined models for predicting intra-tumoral TLSs. (**A**) Nomogram of the combined model for predicting TLSs. (**B**) Forest plot of predictors for TLSs. (**C**) Calibration curves of the nomogram. (**D**) Decision curves analysis of the nomogram.
Abbreviations: LYM, lymphocyte counts; NEUT, neutrophil counts. TLSs, tertiary lymphoid structures.

Table 3 Diagnostic Performance of Different Models

Model	Cohort	AUC (95% CI)	Accuracy	Sensitivity	Specificity	PPV	NPV
Combined model	Training cohort	0.890(0.833,0.947)	0.867	0.882	0.808	0.947	0.636
	Testing cohort	0.857(0.742,0.972)	0.850	0.929	0.667	0.867	0.800
Clinical factors (LYM+satellite nodules)	Training cohort	0.655(0.545,0.764)	0.547	0.490	0.769	0.893	0.278
	Testing cohort	0.719(0.556,0.882)	0.675	0.643	0.750	0.857	0.474
IVIM parameters (f_Maximum+ADC_90Percentile)	Training cohort	0.719(0.620,0.819)	0.680	0.667	0.731	0.907	0.358
	Testing cohort	0.720(0.557,0.883)	0.775	0.857	0.583	0.828	0.636
Radiomics model	Training cohort	0.763(0.672,0.853)	0.828	0.912	0.500	0.877	0.591
	Testing cohort	0.801(0.663,0.938)	0.850	0.964	0.583	0.844	0.875
LYM	Training cohort	0.620(0.506,0.734)	0.555	0.510	0.731	0.881	0.275
	Testing cohort	0.661(0.484,0.838)	0.625	0.571	0.750	0.842	0.429
Satellite nodules	Training cohort	0.557(0.436,0.678)	0.797	0.961	0.154	0.817	0.500
	Testing cohort	0.589(0.400,0.779)	0.425	0.179	1.000	1.000	0.343
f_Maximum	Training cohort	0.608(0.492,0.724)	0.695	0.755	0.462	0.846	0.324
	Testing cohort	0.673(0.498,0.847)	0.775	0.929	0.417	0.788	0.714
ADC_90Percentile	Training cohort	0.610(0.494,0.725)	0.789	0.912	0.308	0.838	0.471
	Testing cohort	0.589(0.400,0.779)	0.725	0.929	0.250	0.743	0.600

Abbreviations: LYM, lymphocyte counts; f, perfusion fraction; ADC, apparent diffusion coefficient; PPV, positive predictive value; NPV, negative predictive value; AUC, area under curve.

prediction and actual observation of TLS status, demonstrating a good fit between the predictions and observations (Figure 5C and D).

In the model comparison, the combined model outperformed both the independent radiomics model, IVIM parameters model, and clinical-radiologic model in the training cohort (AUC, 0.89 vs 0.76, 0.72 and 0.65, respectively) with significant difference (all $p < 0.05$ using DeLong test, Table S4). The combined model showed no significant differences using DeLong test (Table S4), but showed a slight improvement over the other models in the testing cohort (AUC, 0.86 vs 0.80, 0.72 and 0.72, respectively) (Figure 4B and C, Table 3).

Furthermore, the combination of radscores from all IVIM maps outperformed the radscores calculated from individual IVIM maps. The radiomics model that integrated these combined radscores achieved an AUC of 0.76, which was better than the AUC values of the radiomics models based on the Dt, Dp, f, and ADC maps alone for predicting intra-tumoral TLSs in the training cohort. Those individual model AUC values were 0.70, 0.60, 0.60, and 0.59, respectively.

Correlations of TLS Status and the Nomogram with RFS

The median follow-up period for HCC was 30 months (interquartile range (IQR), 16–40 months) for the overall cohort. The median follow-up period was 29.00 months (IQR, 16.00–38.25 months) and 34.50 months (IQR, 15.75–42.00 months) for the training and testing cohorts, respectively. The median RFS was 21 months (IQR, 10–31 months), and 44 out of 168 patients (26.19%) experienced recurrence within two years. The median RFS time of the TLSs- group was 30 months for the training cohort and 32 months for the testing cohort. The TLSs+ group did not reach the median RFS time. TLSs+ group had a low risk of recurrence than that of the TLSs- group ($p = 0.013$, $p < 0.001$, Figure 6A and C).

https://doi.org/10.2147/JHC.S508357

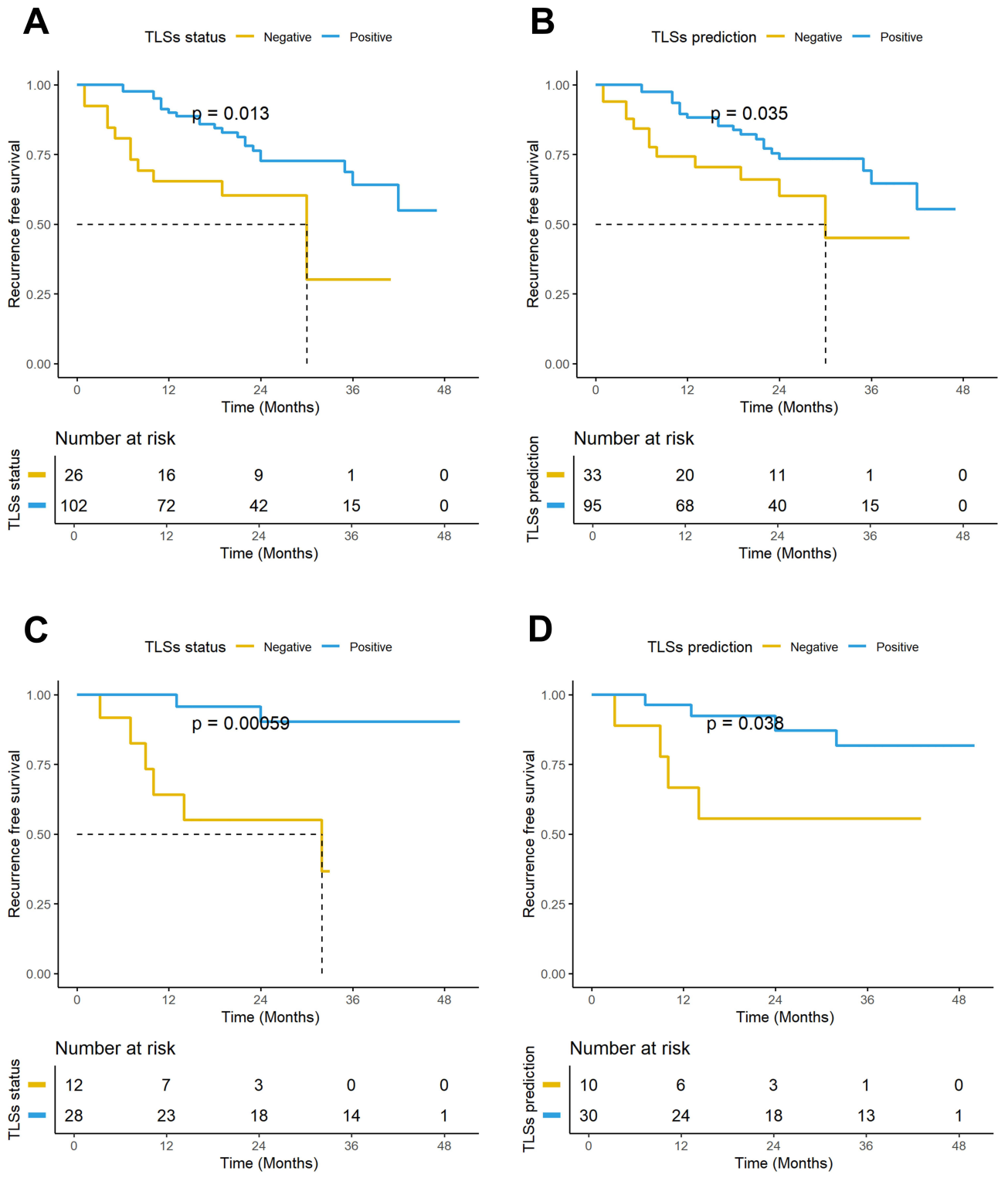

Figure 6 KM curves of early RFS in patients with HCC. KM curves of RFS were stratified based on histologic intra-tumoral TLS status and constructed nomogram score (cutoff value =0.731) in the training (**A, B**), and testing cohorts (**C, D**).

Abbreviations: KM, Kaplan–Meier. RFS, recurrence-free survival. TLSs, tertiary lymphoid structures. HCC, hepatocellular carcinoma.

https://doi.org/10.2147/JHC.S508357

The TLSs predicted by nomogram revealed that the RFS outcomes of the TLSs+ group (cutoff score ≥0.731 based on optimal Youden's index) were also significantly better than those of the TLSs- group (cutoff score <0.731) (p = 0.035, p = 0.038, Figure 6B and D).

Discussion

This study evaluated the value of IVIM parameters, clinical-radiologic features, and radiomics features based on the IVIM sequence in predicting the presence of intra-tumoral TLSs in patients with HCC and developed nomograms by combining these factors. ADC_90Percentile and f_Maximum, satellite nodules, LYM, and radiomics score based on the IVIM sequence exhibited good performance for the prediction of intra-tumoral TLSs in patients with HCC. The combined model demonstrated superior predictive efficacy to those of the remaining models and aided in the precise prediction of intra-tumoral TLSs. Furthermore, the present study demonstrated that the presence of intra-tumoral TLSs was associated with a favorable prognosis and better RFS for HCC, consistent with the findings of previous studies.[24,25]

The use of the IVIM model or IVIM histogram to predict TLSs in HCC or other tumors has not been previously reported. Our results indicated that ADC_90Percentile of the TLSs+ group in HCC was significantly higher and f_Maximum was significantly lower than those of the TLSs- group. ADC is a calculated value that incorporates data regarding tissue cellularity (D) and perfusion (f).[26] The findings of the present study align with those of a previous study,[27] indicating that higher-grade HCC with poorer prognostic outcomes is associated with lower ADC values. HCCs without TLSs are more likely to be poorly differentiated compared to those with TLSs.[9] Well-differentiated HCCs grow with sinusoidal capillarization, which leads to increased vascular permeability and can increase the free water in the extracellular spaces of HCC. Therefore, HCCs with intra-tumoral TLSs usually translate into a more random motion of water molecules and a lower degree of restriction, consistent with our finding that ADC_90Percentile values are higher. The f-value indicates the blood perfusion status and the proportion of capillary blood flow within the tumor.[28] These values are strongly associated with unfavorable prognostic outcomes,[29,30] which may be attributed to the correlation between the malignancy of the tumor and increased microcirculation within the tumor, leading to higher f-values.[31] A previous study showed that the positive rate of vessels encapsulating tumor clusters (VETC) was lower in the TLSs+ group than in the TLSs- group.[13] The microvessel density within the tumor was notably elevated in the VETC+ group compared to the VETC- group,[32] which may explain the lower f_Maximum value in the TLSs+ group compared with the TLSs- group. Imaging histological analysis methods enhance predictive stability during investigations of IVIM-MRI perfusion coefficients, among which f_Maximum could be an effective predictor of intra-tumor TLSs in HCC.

The present study showed that satellite nodules were an independent predictor of intra-tumoral TLSs in HCC. The positivity of TLSs was lower when a satellite focus was present, possibly indicating that the presence of satellite nodules in HCC represents an increased risk of tumor spread and intrahepatic metastasis[33] and a higher risk of MVI.[34] Furthermore, the presence of satellite nodules indicates cancer cell invasion, suggesting an increased risk of recurrence and poorer prognosis.[35]

TLSs rich in B cells can affect immunotherapy responses.[36,37] B cells induce the production of cytotoxic T lymphocytes in TLSs, suggesting a potential role of TLSs in cellular immunity.[38] Moreover, intra-tumoral TLSs are sensitive to immunomodulatory treatments,[39] indicating that B cells and TLSs may enhance immunotherapeutic responses.[40] Therefore, higher LYM may reflect the involvement of intra-tumoral TLSs in cellular immunity, which is consistent with the finding of this study that LYM >1.87×10^8/L was an independent predictor of TLSs.

Tumor heterogeneity, immunophenotyping, and microscopic pathological features may be associated with different radiomics signatures in patients with intrahepatic cholangiocarcinoma[41] and HCC[25] with TLS+ and TLS- status. Therefore, radiomics based on the IVIM sequence were used in our study to predict the TLS status in HCC. These features exhibited preferable prediction ability, which was significantly associated with RFS. The AUC of the combined radscore derived from all the IVIM sequences exhibited notable improvement compared with those of the individual IVIM parameters and radscore derived from each individual IVIM sequence. Therefore, the combined radscore based on all the IVIM sequences may facilitate a more comprehensive and detailed assessment of tissue cellularity and microcirculation.

The combined model comprised cellularity-related ADC value, vascularity-related f-values, invasiveness-related satellite nodules, immune-related LYM, and heterogeneity-related radiomics features. Therefore, the predictive model may simultaneously reflect different tissue properties affected by the occurrence, metastasis, and tumor invasion and achieve a better performance. Radiomics features based on IVIM-DWI provide a more comprehensive representation of microscopic tumor characteristics, including structural composition, blood supply, and intrinsic properties, and can facilitate the assessment of tumor microscopic features.[42,43] The present study demonstrated that IVIM-based parameters may serve as promising biomarkers for identifying intra-tumoral TLSs in HCC. The use of multiple parameters in combined diffusion models may facilitate a comprehensive assessment of tumor characteristics, thereby providing additional information and improving diagnostic accuracy. The RFS curves of the TLSs+ and TLSs- groups predicted by the combined model were similar to the actual RFS curves. Therefore, predicting the presence of intra-tumoral TLSs in patients with HCC using the combined model may guide the clinical management of HCC.

Limitations

The present study had some limitations. First, this was a prospective study, stratifying patients through temporal partitioning to compensate for the limitation of single-center study. Despite the implementation of cross-validation and the internal independent testing cohort, the incorporation of multicenter data with external validation would provide more robust evidence. Second, the present study focused solely on IVIM sequences. Future studies should incorporate additional multiparameter sequences to improve the effectiveness of the proposed model. Lastly, the intra-tumoral TLSs were not quantitatively graded owing to the constraints of the relatively small sample size.

Conclusion

The present study demonstrated that the nomogram incorporating IVIM sequences may serve as a pre-operative predictive biomarker of intra-tumoral TLS status. The RFS of patients with HCC with intra-tumoral TLSs was superior to that of patients without intra-tumoral TLSs.

Abbreviations

ADC, apparent diffusion coefficient; AFP, α-fetoproteinAUC, area under curve; NEUT, neutrophil counts; LYM, lymphocyte counts; BCLC, Barcelona Clinic Liver Cancer; CI, confidence interval; CT, computed tomography; DCA, decision curve analysis; Dp, perfusion related diffusion coefficient; Dt, true diffusion coefficient; DWI, diffusion weighted imaging; f, perfusion fraction; FL, lymphoid follicles; HCC, hepatocellular carcinoma; ICC, intra-class correlation coefficient; IVIM, intravoxel incoherent motion; MRI, magnetic resonance imaging; MVI, microvascular invasion; OR, odds ratio; radscore, radiomic features score; RFS, recurrence-free survival; TLSs, tertiary lymphatic structures; VOI, volume of interest; WSIs, whole pathological slide images.

Key Points

- Predicting intra-tumoral TLSs in HCC in crucial for determining candidates for immunotherapy.
- Nomograms combining IVIM parameters, clinical-radiologic, and radiomics features are potential TLS-status biomarkers.
- Intra-tumoral TLSs were associated with favorable prognoses and better recurrence-free survival.

Data Sharing Statement

For scientific reasons, raw data may be obtained with the permission of the corresponding author.

Ethics Approval and Consent to Participate

This prospective study was approved by the Institutional Review Board of Sun-Yat Sen University Cancer Center (B2019-187-01). Written informed consent was obtained from all the participants.

Consent for Publication

Written informed consent was obtained from all the participants. All presentations of case reports have consent to publish.

Funding

This study was supported by grants from the National Natural Science Foundation of China (No. 82471944) and Guangdong Medical Science and Technology Research Foundation (A2024578).

Disclosure

Xiaolan Zhang and Jing Hu are affiliated with Shukun Technology. Yunfei Zhang is affiliated with United Imaging Healthcare. All authors have no other conflicts of interest to declare related to this article.

References

1. Craig AJ, von Felden J, Garcia-Lezana T. et al. Tumour evolution in hepatocellular carcinoma. *Nat Rev Gastroenterol Hepatol*. 2020;17(3):139–152. doi:10.1038/s41575-019-0229-4
2. Saito A, Toyoda H, Kobayashi M, et al. Prediction of early recurrence of hepatocellular carcinoma after resection using digital pathology images assessed by machine learning. *Mod Pathol*. 2021;34(2):417–425. doi:10.1038/s41379-020-00671-z
3. Sangro B, Melero I, Wadhawan S, et al. Association of inflammatory biomarkers with clinical outcomes in nivolumab-treated patients with advanced hepatocellular carcinoma. *J Hepatol*. 2020;73(6):1460–1469. doi:10.1016/j.jhep.2020.07.026
4. Sautès-Fridman C, Petitprez F, Calderaro J, Fridman WH. Tertiary lymphoid structures in the era of cancer immunotherapy. *Nat Rev Cancer*. 2019;19(6):307–325. doi:10.1038/s41568-019-0144-6
5. Sautès-Fridman C, Lawand M, Giraldo NA, et al. Tertiary lymphoid structures in cancers: prognostic value, regulation, and manipulation for therapeutic intervention. *Front Immunol*. 2016;7. doi:10.3389/fimmu.2016.00407
6. Fridman WH, Zitvogel L, Sautès-Fridman C, Kroemer G. The immune contexture in cancer prognosis and treatment. *Nat Rev Clin Oncol*. 2017;14(12):717–734. doi:10.1038/nrclinonc.2017.101
7. Helmink BA, Reddy SM, Gao J, et al. B cells and tertiary lymphoid structures promote immunotherapy response. *Nature*. 2020;577(7791):549–555. doi:10.1038/s41586-019-1922-8
8. Calderaro J, Petitprez F, Becht E, et al. Intra-tumoral tertiary lymphoid structures are associated with a low risk of early recurrence of hepatocellular carcinoma. *J Hepatol*. 2019;70(1):58–65. doi:10.1016/j.jhep.2018.09.003
9. Li H, Liu H, Fu H, et al. Peritumoral tertiary lymphoid structures correlate with protective immunity and improved prognosis in patients with hepatocellular carcinoma. *Front Immunol*. 2021;12:648812. doi:10.3389/fimmu.2021.648812
10. Posch F, Silina K, Leibl S, et al. Maturation of tertiary lymphoid structures and recurrence of stage II and III colorectal cancer. *Oncoimmunology*. 2018;7(2):e1378844. doi:10.1080/2162402X.2017.1378844
11. Sun R, Limkin EJ, Vakalopoulou M, et al. A radiomics approach to assess tumour-infiltrating CD8 cells and response to anti-PD-1 or anti-PD-L1 immunotherapy: an imaging biomarker, retrospective multicohort study. *Lancet Oncol*. 2018;19(9):1180–1191. doi:10.1016/S1470-2045(18)30413-3
12. Sun L, Mu L, Zhou J, et al. Imaging features of gadoxetic acid-enhanced MR imaging for evaluation of tumor-infiltrating CD8 cells and PD-L1 expression in hepatocellular carcinoma. *Cancer Immunol Immunother*. 2022;71(1):25–38. doi:10.1007/s00262-021-02957-w
13. Li P, Liang Y, Zeng B, et al. Preoperative prediction of intra-tumoral tertiary lymphoid structures based on CT in hepatocellular cancer. *Eur J Radiol*. 2022;151:110309. doi:10.1016/j.ejrad.2022.110309
14. Meeus EM, Zarinabad N, Manias KA, et al. Diffusion-weighted MRI and intravoxel incoherent motion model for diagnosis of pediatric solid abdominal tumors. *J Magn Reson Imaging*. 2018;47(6):1475–1486. doi:10.1002/jmri.25901
15. Peng J, Zheng J, Yang C, et al. Intravoxel incoherent motion diffusion-weighted imaging to differentiate hepatocellular carcinoma from intrahepatic cholangiocarcinoma. *Sci Rep*. 2020;10(1):7717. doi:10.1038/s41598-020-64804-9
16. Noda Y, Goshima S, Fujimoto K, et al. Comparison of the diagnostic value of mono-exponential, bi-exponential, and stretched exponential signal models in diffusion-weighted MR imaging for differentiating benign and malignant hepatic lesions. *Magn Reson Med Sci*. 2021;20(1):69–75. doi:10.2463/mrms.mp.2019-0151
17. Wei Y, Gao F, Wang M, et al. Intravoxel incoherent motion diffusion-weighted imaging for assessment of histologic grade of hepatocellular carcinoma: comparison of three methods for positioning region of interest. *Eur Radiol*. 2019;29(2):535–544. doi:10.1007/s00330-018-5638-1
18. Wei Y, Huang Z, Tang H, et al. IVIM improves preoperative assessment of microvascular invasion in HCC. *Eur Radiol*. 2019;29(10):5403–5414. doi:10.1007/s00330-019-06088-w
19. Li Q, Zhang T, Che F, et al. Intravoxel incoherent motion diffusion weighted imaging for preoperative evaluation of liver regeneration after hepatectomy in hepatocellular carcinoma. *Eur Radiol*. 2023. doi:10.1007/s00330-023-09496-1
20. Jia F, Wu B, Yan R, et al. Prediction model for intermediate-stage hepatocellular carcinoma response to transarterial chemoembolization. *J Magn Reson Imaging*. 2020;52(6):1657–1667. doi:10.1002/jmri.27189
21. Zhou Y, Zheng J, Yang C, et al. Application of intravoxel incoherent motion diffusion-weighted imaging in hepatocellular carcinoma. 2022;28.
22. Finkin S, Yuan D, Stein I, et al. Ectopic lymphoid structures function as microniches for tumor progenitor cells in hepatocellular carcinoma. *Nat Immunol*. 2015;16(12):1235–1244. doi:10.1038/ni.3290
23. van Griethuysen JJM, Fedorov A, Parmar C, et al. Computational radiomics system to decode the radiographic phenotype. *Cancer Res*. 2017;77(21):e104–e107. doi:10.1158/0008-5472.CAN-17-0339

24. Ding G-Y, Ma J-Q, Yun J-P, et al. Distribution and density of tertiary lymphoid structures predict clinical outcome in intrahepatic cholangiocarcinoma. *J Hepatol*. 2022;76(3):608–618. doi:10.1016/j.jhep.2021.10.030
25. Shu DH, Ho WJ, Kagohara LT. Immunotherapy response induces divergent tertiary lymphoid structure morphologies in hepatocellular carcinoma. *Nat Immunol*. 2024;25(11):2110–2123. doi:10.1038/s41590-024-01992-w
26. Chandarana H, Lee VS, Hecht E, et al. Comparison of biexponential and monoexponential model of diffusion weighted imaging in evaluation of renal lesions: preliminary experience. *Invest Radiol*. 2011;46(5):285–291. doi:10.1097/RLI.0b013e3181ffc485
27. Woo S, Lee JM, Yoon JH, et al. Intravoxel incoherent motion diffusion-weighted MR imaging of hepatocellular carcinoma: correlation with enhancement degree and histologic grade. *Radiology*. 2014;270(3):758–767. doi:10.1148/radiol.13130444
28. Choi S-Y, Kim SH, Park CK, et al. Imaging features of gadoxetic acid-enhanced and diffusion-weighted MR imaging for identifying cytokeratin 19-positive hepatocellular carcinoma: a retrospective observational study. *Radiology*. 2018;286(3):897–908. doi:10.1148/radiol.2017162846
29. Ningning D, Haopeng P, Xuefei D, et al. Perfusion imaging of brain gliomas using arterial spin labeling: correlation with histopathological vascular density in MRI-guided biopsies. *Neuroradiology*. 2017;59(1):51–59. doi:10.1007/s00234-016-1756-0
30. Lemke A, Laun FB, Simon D, et al. An in vivo verification of the intravoxel incoherent motion effect in diffusion-weighted imaging of the abdomen. *Magn Reson Med*. 2010;64(6):1580–1585. doi:10.1002/mrm.22565
31. Zhang Y, Liu L, Zhang K, et al. Nomograms Combining Clinical and Imaging Parameters to Predict Recurrence and Disease-free Survival After Concurrent Chemoradiotherapy in Patients With Locally Advanced Cervical Cancer. *Acad Radiol*. 2023;30(3):499–508. doi:10.1016/j.acra.2022.08.002
32. Huang C-W, Lin S-E, Huang S-F, et al. The Vessels That Encapsulate Tumor Clusters (VETC) pattern is a poor prognosis factor in patients with hepatocellular carcinoma: an analysis of microvessel density. *Cancers*. 2022;14(21):5428. doi:10.3390/cancers14215428
33. Kim S, Shin J, Kim D-Y, et al. Radiomics on gadoxetic acid-enhanced magnetic resonance imaging for prediction of postoperative early and late recurrence of single hepatocellular carcinoma. *Clin Cancer Res*. 2019;25(13):3847–3855. doi:10.1158/1078-0432.CCR-18-2861
34. Zhou L, Qu Y, Quan G, et al. Nomogram for predicting microvascular invasion in hepatocellular carcinoma using gadoxetic acid-enhanced MRI and intravoxel incoherent motion imaging. *Acad Radiol*. 2023;S1076-6332(23):335. doi:10.1016/j.acra.2023.06.028
35. Xue R, Li R, Guo H, et al. Variable intra-tumor genomic heterogeneity of multiple lesions in patients with hepatocellular carcinoma. *Gastroenterology*. 2016;150(4):998–1008. doi:10.1053/j.gastro.2015.12.033
36. Fridman WH, Meylan M, Petitprez F, et al. B cells and tertiary lymphoid structures as determinants of tumour immune contexture and clinical outcome. *Nat Rev Clin Oncol*. 2022;19(7):441–457. doi:10.1038/s41571-022-00619-z
37. Laumont CM, Banville AC, Gilardi M, et al. Tumour-infiltrating B cells: immunological mechanisms, clinical impact and therapeutic opportunities. *Nat Rev Cancer*. 2022;22(7):414–430. doi:10.1038/s41568-022-00466-1
38. Yamakoshi Y, Tanaka H, Sakimura C, et al. Immunological potential of tertiary lymphoid structures surrounding the primary tumor in gastric cancer. *Int J Oncol*. 2020;57(1):171–182. doi:10.3892/ijo.2020.5042
39. Johansson-Percival A, He B, Li Z-J, et al. De novo induction of intratumoral lymphoid structures and vessel normalization enhances immunotherapy in resistant tumors. *Nat Immunol*. 2017;18(11):1207–1217. doi:10.1038/ni.3836
40. Wang M, Zadeh S, Pizzolla A, et al. Characterization of the treatment-naive immune microenvironment in melanoma with BRAF mutation. *J Immunother Cancer*. 2022;10(4):e004095. doi:10.1136/jitc-2021-004095
41. Xu Y, Li Z, Yang Y, et al. Association between MRI radiomics and intratumoral tertiary lymphoid structures in intrahepatic cholangiocarcinoma and its prognostic significance. *Magnetic Resonance Imag*. 2023:jmri.29128. doi:10.1002/jmri.29128.
42. Li C, Zheng M, Zheng X, et al. Predictive Ki-67 proliferation index of cervical squamous cell carcinoma based on IVIM-DWI combined with texture features. *Contrast Media mol Imaging*. 2021;2021:8873065. doi:10.1155/2021/8873065
43. Zheng X, Li C, Zhang L, et al. Combining intravoxel incoherent motion diffusion weighted imaging and texture analysis for a nomogram to predict early treatment response to concurrent chemoradiotherapy in cervical cancer patients. *J Oncol*. 2021;2021:9345353. doi:10.1155/2021/9345353